

Investigation on calibration methods for multi-axis, linear and redundant force sensors

C M Oddo¹, P Valdastrì², L Beccai³, S Roccella³, M C Carrozza³
and P Dario^{2,3}

¹ Scuola Superiore Sant'Anna, Piazza Martiri della Libertà 33, 56127 Pisa, Italy

² CRIM Lab, Scuola Superiore Sant'Anna, v.le R Piaggio 34, 56025 Pontedera (PI), Italy

³ ARTS Lab, Scuola Superiore Sant'Anna, v.le R Piaggio 34, 56025 Pontedera (PI), Italy

E-mail: oddoc@sssup.it and valdastrì@sssup.it

Received 5 October 2006, in final form 20 November 2006

Published 19 January 2007

Online at stacks.iop.org/MST/18/623

Abstract

A new method for the calibration of multi-axis, linear and redundant force sensors is presented. This new procedure, named device hyperplane characterization method, is inspired by the *shape from motion method* for it reduces the burden represented by the need for a huge number of force measurements, typical using least-squares methods, in order to reject errors during the calibration procedure. The proposed technique is an application of the rank theorem and achieves good noise rejection without much time consumption focusing on sensor output measurements, and reducing the effect of disturbances operating the projection of raw output data on the hyperplane to which measurements are ideally compelled to belong in the case of redundant sensors.

Keywords: triaxial force sensor, calibration, linear, redundant, hyperplane

(Some figures in this article are in colour only in the electronic version)

1. Introduction

Force sensor calibration procedures have to be accurate and time effective. Traditional least-squares calibration methods perform with high accuracy [1, 2], but outputs recording require the precise application of a wide set of known forces carefully selected to adequately span the space of the sensor [3, 4]. The *shape from motion method* [3, 5] performs with accuracy comparable to traditional least-squares methods, but eliminates the need for explicit knowledge of all the applied load vectors, yielding fast and precise calibration results. In such a method [3], a constant-magnitude force (a mass in a gravity field [6]) is randomly moved through the sensing space of the sensor while raw data are continuously gathered. Operating singular value decomposition, the calibration matrix of the sensor is calculated by using only one known force, thus reducing the burden of data collection for applied forces. Besides, such an approach is efficient if the maximum force applicable to the sensor does not depend on its direction. In that

case the external stimulus can be provided by simply attaching a compact proof mass to the end effector of the device. Differently, if force limits vary with respect to the direction of the force, two solutions may be considered: building a physical bond which would produce an adequate non-spherical force distribution or, alternatively, using a spherical distributed stimulus attaching a proof mass upper limited by the minimum applicable force. Both these operations have limitations: in the first case building a non-spherical force distribution may be a complex operation, and the second solution may be inadequate due to the reduced applied force (at least in one direction) with respect to the full-scale one.

In this work, a new force sensor characterization method is proposed. The procedure has been proved to be accurate and time effective for a linear and redundant (i.e. higher number of transducers with respect to the unknown load components [7]) triaxial force sensor having a cylindrical working range. The method, reported in section 4.1, is tested on a force sensor belonging to the family described in [8], which was

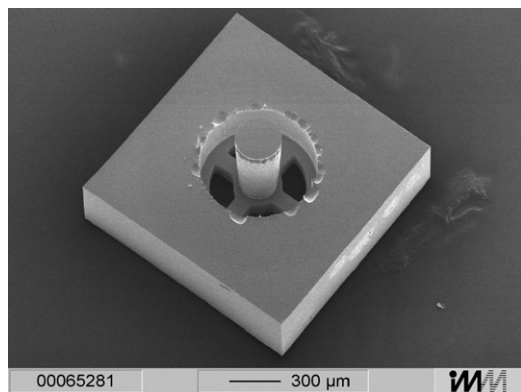


Figure 1. SEM image of the sensing chip.

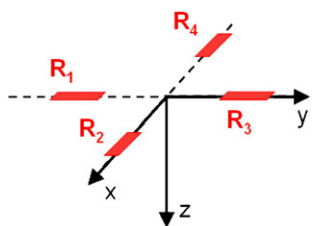


Figure 2. Piezoresistor orientations with respect to the chosen reference system.

characterized in [9] using a traditional *least-squares method*. The main idea of this new procedure is to characterize the range space of the sensor calibration matrix since the investigated device is linear and redundant, and so output data have to belong [7] to a hyperplane of \mathbb{R}^4 ; hyperplane characterization is a time effective output focused operation, given that it does not require any knowledge of applied forces. Only three force measurements are strictly needed in order to obtain calibration matrices with good noise immunity, thanks to the operation of projecting raw output data on the characteristic hyperplane of the sensor. In section 4.4, results obtained in such a way are compared to those achieved using *least-squares methods*, which are summarized in section 3.6. This new method, as outlined in sections 4 and 5, is also useful to automatically check if the device is working properly (i.e. according to the previously performed characterization) in its structured environment [1, 2, 10, 11] without the need to apply known forces to the sensor.

2. Sensor description and calibration setup

The sensor investigated in this work has been presented in [8, 12], and characterized in [9] using a *least-squares procedure*. It is a redundant [7] triaxial force sensor. It consists of a sensing chip (figures 1 and 2) that comprises four tethers whose axes are perpendicular to each other, and a cylinder, located at the centre, which transmits the force. Four bar shape p-type piezoresistors (figure 3), positioned in high stress areas of the bottom side, are used independently in order to measure the three components of an applied force through *fractional changes in resistance*. Therefore, the three components of an external force, applied on the cylinder, can be obtained from the four *fractional changes in resistance* of

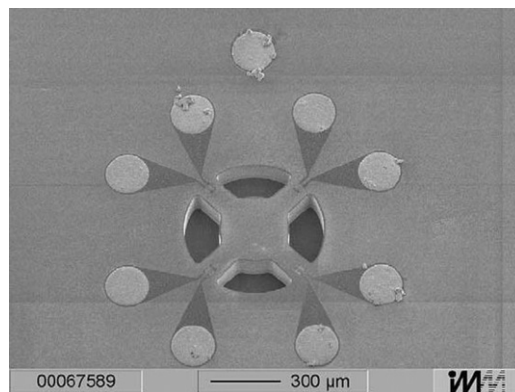


Figure 3. Bottom side of the sensor, showing the four piezoresistor locations.

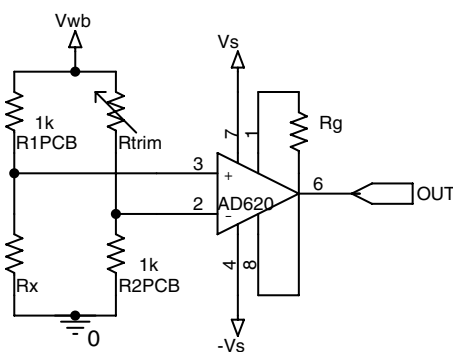


Figure 4. Schematic view of the signal conditioning electronics.

the piezoresistors implanted in each tether. In particular, a normal force will result in a uniform variation of the all four *fractional changes in resistance*, while a tangential force, e.g. directed along the X-axis of figure 2 will determine opposite behaviour of the *fractional changes in resistance* of R_2 and R_4 , while it will not affect R_1 and R_3 .

The sensor, whose dimensions are $1.5 \text{ mm} \times 1.5 \text{ mm} \times 0.65 \text{ mm}$, is connected to a carrier chip by flip chip bonding. In this way the device can be connected to the external instrumentation by means of wire bonding. The conditioning electronics (figure 4) is the same as described in [8]: each piezoresistor (R_X , where $X = 1, \dots, 4$) is independently conditioned using a quarter Wheatstone bridge configuration, composed by two precision $1 \text{ k}\Omega$ resistors and one trimmer, in order to adjust the initial offset level. The bridge output signal is led to an instrumentation amplifier (AD620, Analog Devices, Norwood, MA, USA) which converts the signal from differential to single ended and provides a gain $A = 420$. Considering a balanced bridge (i.e. at the bias point $R_{1PCB} = R_{2PCB} = R_{trim} = R_X = R$), the output of the circuit is

$$V_{OUT} = A \cdot V_{wb} \cdot \frac{\Delta R}{4R + 2\Delta R} \approx A \cdot V_{wb} \frac{\Delta R}{4R}. \quad (1)$$

The resistance variation ΔR of each piezoresistor can be obtained once the output voltage V_{OUT} of each channel is known. Data acquisition is performed using a DAQ Card (NI 6062E, from National Instruments, Austin, TX, USA) while operating load–unload cycles to the sensor as presented later in section 3.2 using the test bench described in [9].

3. Characterization methodology

3.1. Theoretical considerations

The main purpose of this work is to investigate the methodology that can be applied in order to obtain a functional relation between input and output of a linear redundant [7] triaxial force sensor. From a systemic point of view, the input applied to the sensor is the force vector \underline{F} , and the output is the vector \underline{R} of four fractional changes in resistance, obtained from the voltages collected between two nodes of each Wheatstone bridge:

$$\underline{F} = \begin{pmatrix} F_x \\ F_y \\ F_z \end{pmatrix} \quad (2)$$

$$\underline{R} = \begin{pmatrix} \frac{\Delta R_1}{R_1} \\ \frac{\Delta R_2}{R_2} \\ \frac{\Delta R_3}{R_3} \\ \frac{\Delta R_4}{R_4} \end{pmatrix}. \quad (3)$$

The functional relation which describes the behaviour of the sensor may be represented using the application $\beta : \mathbb{R}^3 \rightarrow \mathbb{R}^4$, where \mathbb{R}^3 is the space of force vectors, and \mathbb{R}^4 that of fractional changes in resistance. Assuming that a linear relation between input and output exists, the function β may be represented with a compliance matrix within the working range of the sensor.

Although from a physical point of view the input signal is the applied force, and the output is the vector of fractional changes in resistance, from a functional perspective the sensor would be used to recognize the input force. This theoretical symmetry allows us to consider the vector of forces as an independent variable, and the vector of fractional changes in resistance as a dependent variable, or vice versa. In the latter case, since the sensor is redundant, fractional changes in resistance vectors have a constraint because they ideally belong to a hyperplane of \mathbb{R}^4 . Those two opposite points of view give the two linear relations (4) and (5), where \underline{B} is a uniquely determined 4×3 matrix (the aim is to evaluate it, according to a certain optimum criterion), and \underline{A} is a 3×4 one (\underline{A} matrix can be chosen in various suitable ways, as explained in section 3.3.3):

$$\underline{F} = \underline{A} \cdot \underline{R} \quad (4)$$

$$\underline{R} = \underline{B} \cdot \underline{F}. \quad (5)$$

3.2. Characterization protocol

The protocol used to characterize the sensor gives a fixed number of measurements near each point of a discrete set of values of applied forces. A force is said to belong to the load scheme X , Y or Z if F_x , F_y or F_z is much greater than the two remaining components, respectively.

When a force is applied during the characterization session, the test bench is used in such a way to guarantee that the applied force pertains to a certain load scheme, having a set of measurements with $F_x \gg F_y$ and $F_x \gg F_z$, or $F_y \gg F_x$ and $F_y \gg F_z$, or $F_z \gg F_x$ and $F_z \gg F_y$. In this way, if forces

belong to load schemes X , Y and Z , the \mathbb{R}^3 space could be generated by linear composition of the imposed force vectors, and the problem is not badly conditioned, thanks to the quasi-orthogonality of vectors belonging to different load schemes. Due to the inevitable imperfect alignment between the axis of the load cell, and the loaded axis of the sensor, during load scheme Z , F_x and F_y are not null even if they are much lower than F_z . The same phenomenon happens during load scheme X or Y . This does not represent a problem because the load cell is a three-axial one, and all three force components are acquired during characterization.

Forces belonging to the load scheme Z have F_z between 0 N and 2.5 N, while in load schemes X and Y , F_x and F_y are between 0 N and 0.25 N. This is the reason why the shape from motion method could not be easily applied to this kind of sensor. In fact, if a spherical stimulus in the space of forces is used, its modulus cannot be greater than 0.25 N. Alternatively, the whole working range of the sensor can be explored using another kind of force distribution in the space of forces (for example an elliptical one), but this operation could be very difficult, given that a geometrical bond has to be built in order to be sure that the distribution of forces is the expected one.

Each measurement is composed by a load-unload cycle: data with both the sensor loaded and unloaded are saved. During the post-processing phase, the difference between each load and unload measurement is made, in order to minimize the offset vector without spending much time regulating the trimmer of each Wheatstone bridge. In the following sections, $Q (= 36)$ is the total number of measurements.

3.3. Data interpolation methods

3.3.1. Least-squares solution. In order to obtain the 12 coefficients of the matrix \underline{B} , 12 independent equations are needed. In the ideal (errorless) case, the interpolation problem is to find the matrix \underline{B} which solves, for all i , the equation $\underline{R}^i = \underline{B} \cdot \underline{F}^i$, where \underline{R}^i and \underline{F}^i are the vector of fractional changes in resistance and forces measured during the i th relevation overall Q , respectively. To obtain 12 independent equations, three independent forces have to be applied. As previously mentioned, the number of measurements Q was 36, in order to achieve a satisfactory trade-off between the error rejection and the data collection time expense.

In this case, since $Q > 3$, the solution can be in the least-squares meaning, and it is achieved in the following through the standard regression technique, described by the relations:

$$\underline{B}_{\text{LSM}} = \underline{R} \cdot \underline{F}^T \cdot (\underline{F} \cdot \underline{F}^T)^{-1}. \quad (6)$$

T is the transposition operator; \underline{F} and \underline{R} are the matrices containing the $3 \times Q$ force and the $4 \times Q$ fractional changes in resistance measurements, respectively:

$$\underline{F} = \begin{pmatrix} F_x^1 & \dots & F_x^Q \\ F_y^1 & \dots & F_y^Q \\ F_z^1 & \dots & F_z^Q \end{pmatrix} \quad \underline{R} = \begin{pmatrix} R_1^1 & \dots & R_1^Q \\ R_2^1 & \dots & R_2^Q \\ R_3^1 & \dots & R_3^Q \\ R_4^1 & \dots & R_4^Q \end{pmatrix}. \quad (7)$$

3.3.2. *Normalized least-squares solution.* The least-squares method minimizes the canonic 2-norm of the residuals matrix (i.e. $\underline{R} - \underline{B}_{\text{LSM}} \cdot \underline{F}$), but it does not minimize parameters based on relative error because it overestimates data having higher modulus. For the sensor inspected in this work, the range of variability of F_Z is ten times greater than those of F_X and F_Y . In order to take more care of relative error than of absolute error, the matrix $\underline{B}_{\text{NLSM}}$ has also been calculated on the same data set with the least-squares method, applying the following normalization:

$$\underline{F} \rightarrow \underline{F}_n = \begin{pmatrix} \frac{F_X^1}{\sqrt{(F_X^1)^2 + (F_Y^1)^2 + (F_Z^1)^2}} & \cdots & \frac{F_X^Q}{\sqrt{(F_X^Q)^2 + (F_Y^Q)^2 + (F_Z^Q)^2}} \\ \vdots & \vdots & \vdots \\ \frac{F_Z^1}{\sqrt{(F_X^1)^2 + (F_Y^1)^2 + (F_Z^1)^2}} & \cdots & \frac{F_Z^Q}{\sqrt{(F_X^Q)^2 + (F_Y^Q)^2 + (F_Z^Q)^2}} \end{pmatrix} \quad (8)$$

$$\underline{R} \rightarrow \underline{R}_n = \begin{pmatrix} \frac{R_1^1}{\sqrt{(F_X^1)^2 + (F_Y^1)^2 + (F_Z^1)^2}} & \cdots & \frac{R_1^Q}{\sqrt{(F_X^Q)^2 + (F_Y^Q)^2 + (F_Z^Q)^2}} \\ \vdots & \vdots & \vdots \\ \frac{R_4^1}{\sqrt{(F_X^1)^2 + (F_Y^1)^2 + (F_Z^1)^2}} & \cdots & \frac{R_4^Q}{\sqrt{(F_X^Q)^2 + (F_Y^Q)^2 + (F_Z^Q)^2}} \end{pmatrix} \quad (9)$$

3.3.3. *Pseudoinversion.* In order to obtain an \underline{A} matrix, Moore–Penrose pseudoinversion is applied, since \underline{A} is not uniquely determined. In fact, the matrix \underline{B} transforms the space of forces \mathbb{R}^3 into the space of *fractional changes in resistance* $\underline{B}(\mathbb{R}^3)$, which is a hyperplane in \mathbb{R}^4 . The matrix \underline{B} can be inverted from $\underline{B}(\mathbb{R}^3)$ to \mathbb{R}^3 , but not from \mathbb{R}^4 to \mathbb{R}^3 .

Let us call $\underline{A}_1 : \underline{B}(\mathbb{R}^3) \rightarrow \mathbb{R}^3$ the inverse of \underline{B} . In a theoretical situation, the fact that the inversion of \underline{B} is well defined only from $\underline{B}(\mathbb{R}^3)$ would not represent a problem, given that ideally the sensor should return only *fractional changes in resistance* vectors belonging to the hyperplane $\underline{B}(\mathbb{R}^3)$. Nevertheless, dealing with real data, this does not happen, due to noise, experimental errors and negligible nonlinearities of the sensor. Thus, *fractional changes in resistance* vectors could not belong to the hyperplane $\underline{B}(\mathbb{R}^3)$, as represented in figure 5 for a simplified imaginary \mathbb{R}^2 situation. In general, those vectors will form an angle with the hyperplane $\underline{B}(\mathbb{R}^3)$ which would be as little as noise, experimental errors and nonlinearities are limited. The matrix \underline{A} can be defined as a *pseudoinverse* of \underline{B} and written as the product of the two rank-3 matrices $\underline{M} : \mathbb{R}^4 \rightarrow \underline{B}(\mathbb{R}^3)$ and \underline{A}_1 , where \underline{M} is a projection matrix over the hyperplane $\underline{B}(\mathbb{R}^3)$, thus obtaining $\underline{A} = \underline{A}_1 \cdot \underline{M} : \mathbb{R}^4 \rightarrow \mathbb{R}^3$. In particular, \underline{A} and \underline{A}_1 are numerically the same matrix, but formally they are different because they represent linear applications having different domains. As introduced in section 3.3.1 or 3.3.2, $\underline{B}_{\text{LSM}}$ and $\underline{B}_{\text{NLSM}}$ can be used as an estimation of \underline{B} . Then, $\underline{A}_{\text{LSM}}$ and $\underline{A}_{\text{NLSM}}$ can be calculated through the Moore–Penrose pseudoinversion of $\underline{B}_{\text{LSM}}$ and $\underline{B}_{\text{NLSM}}$ respectively.

It is useful at this point to remark that, since \underline{B} is injective, a *pseudoinverse* of \underline{B} is a left inverse of \underline{B} , i.e. a matrix $\underline{A} : \mathbb{R}^4 \rightarrow \mathbb{R}^3$ such that $\underline{A} \cdot \underline{B} = \underline{I}_3$ (where \underline{I}_3 is the identical 3×3 matrix). The Moore–Penrose pseudoinversion calculates

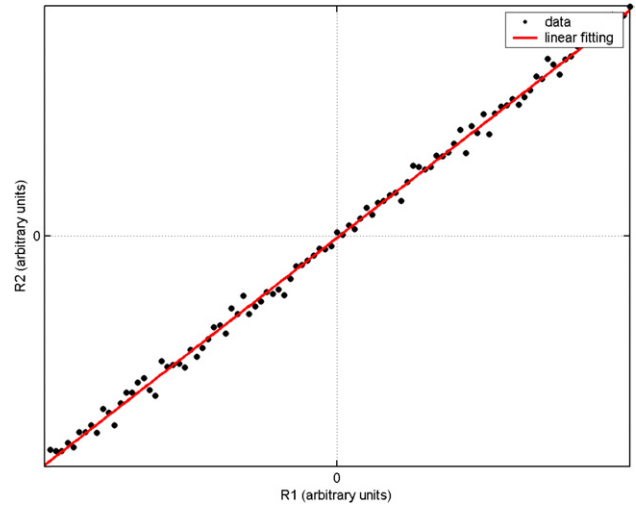


Figure 5. 2D simplification of the hyperplane bond.

\underline{A} such that $\underline{B} \cdot \underline{A} = \underline{M}$ is the orthogonal projection of a vector of \mathbb{R}^4 over the hyperplane $\underline{B}(\mathbb{R}^3)$. The possibility of estimating \underline{M} without previous knowledge of \underline{A} and \underline{B} will be used in section 4 to introduce the new calibration method.

3.4. Compliance matrix regularities

As pointed out in [9], and confirmed here in section 3.6, coefficients of each (supposed) good estimated matrix \underline{B} have the following characteristics: $|b_{2,1}|$ and $|b_{4,1}|$, belonging to the first column of each matrix, are at least one order of magnitude higher than $|b_{1,1}|$ and $|b_{3,1}|$. This is due to the mechanical and technological characteristics of the sensor [8, 12], given that the sensor cross-shape guarantees the mechanical decoupling of the shear components of the applied load, and the transversal sensitivity of each piezoresistor is much lower than its longitudinal one. Moreover, $b_{2,1}$ and $b_{4,1}$ are opposite in sign, due to the fact that a force applied along the X -axis causes tension in piezoresistor R_2 and compression in R_4 or vice versa, according to force orientation. The same regularities can be found considering the second column of each matrix \underline{B} , observing that $|b_{1,2}|$ and $|b_{3,2}|$ are much greater than $|b_{2,2}|$ and $|b_{4,2}|$, and that $b_{1,2}$ and $b_{3,2}$ are opposite in sign. The coefficients of the last column, instead, have the same sign, and all have almost the same magnitude, given that a force belonging to the Z -axis ideally stresses the sensor in a symmetrical way. Similar regularities can be highlighted observing the rows of each matrix \underline{A} , obtained applying the pseudoinversion operator to \underline{B} .

3.5. Error parameters

In order to evaluate the error due to noise, experimental problems and second-order effects, some parameters have to be defined.

Let us define the i th modelled *fractional changes in resistance* vector as $R_{\text{mod}}^i = \underline{B} \cdot F_{\text{meas}}^i$, where F_{meas}^i is the real i th vector of force, measured using the ATI Nano17 F/T transducer. In the same way, the modelled force can be defined as $F_{\text{mod}}^i = \underline{A} \cdot R_{\text{meas}}^i$, where R_{meas}^i is the real i th

Table 1. Force and fractional changes in resistance error parameters using the least-squares method (LSM) and the normalized least squares method (NLSM), as described in sections 3.3.1 and 3.3.2. For force ranges see section 3.2.

	rms($\ \Delta F\ $)	rms($\frac{\ \Delta F\ }{\ F\ }$)	mean($\ \Delta F\ $)	mean($\frac{\ \Delta F\ }{\ F\ }$)	std($\ \Delta F\ $)	std($\frac{\ \Delta F\ }{\ F\ }$)	mean(α_F)	std($ \alpha_F $)
LSM	0.009 08 N	9.6%	0.008 29 N	7.57%	0.003 71 N	5.91%	3.28°	6.8°
NLSM	0.009 66 N	8.77%	0.008 6 N	7.22%	0.004 4 N	4.97%	3.13°	5.37°
	rms($\ \Delta R\ $)	rms($\frac{\ \Delta R\ }{\ R\ }$)	mean($\ \Delta R\ $)	mean($\frac{\ \Delta R\ }{\ R\ }$)	std($\ \Delta R\ $)	std($\frac{\ \Delta R\ }{\ R\ }$)	mean(α_R)	std($ \alpha_R $)
LSM	0.001 22	9.13%	0.001 11	7.52%	0.000 511	5.18%	3.34°	5.69°
NLSM	0.001 34	8.71%	0.001 18	7.43%	0.000 637	4.55%	3.2°	4.1°

vector of fractional changes in resistance, measured using the conditioning electronics, and the data acquisition system, as described in section 2.

According to the kind (force or fractional changes in resistance) of input chosen, we can define the residual vector as $\Delta R^i = R_{\text{mod}}^i - R_{\text{meas}}^i$ or $\Delta F^i = F_{\text{mod}}^i - F_{\text{meas}}^i$. Some relevant error parameters are

$$\text{rms}\left(\frac{\|\Delta R\|}{\|R_{\text{meas}}\|}\right) = \sqrt{\frac{\sum_{i=1}^Q \frac{\|\Delta R^i\|^2}{\|R_{\text{meas}}^i\|^2}}{Q}} \quad (10)$$

$$\text{mean}\left(\frac{\|\Delta R\|}{\|R_{\text{meas}}\|}\right) = \frac{\sum_{i=1}^Q \frac{\|\Delta R^i\|}{\|R_{\text{meas}}^i\|}}{Q} \quad (11)$$

$$\text{std}\left(\frac{\|\Delta R\|}{\|R_{\text{meas}}\|}\right) = \sqrt{\text{rms}^2\left(\frac{\|\Delta R\|}{\|R_{\text{meas}}\|}\right) - \text{mean}^2\left(\frac{\|\Delta R\|}{\|R_{\text{meas}}\|}\right)} \quad (12)$$

where rms means *root mean square*. Analogously, also absolute error parameters are defined, considering rms ($\|\Delta R\|$), mean($\|\Delta R\|$) and std($\|\Delta R\|$). The same parameters can be defined with respect to force error vectors.

These parameters describe the error (absolute or relative) linked to the norm of the mismatch between the measured force and the modelled one.

It is useful to evaluate also the difference between the direction of the real force and the modelled one, introducing parameters that describe the error in terms of the angle $\cos \alpha_F = \langle F_{\text{meas}}^i, F_{\text{mod}}^i \rangle \cdot (\|F_{\text{meas}}^i\| \cdot \|F_{\text{mod}}^i\|)^{-1}$ between those two i th forces, where $0^\circ \leq \alpha_F \leq 180^\circ$, and $\langle \#, \# \rangle$ means inner product. The mean value and the standard deviation of that angle are calculated:

$$\text{mean}(\alpha_F) = \frac{\sum_{i=1}^Q \alpha_F^i}{Q} \quad (13)$$

$$\text{std}(\alpha_F) = \sqrt{\frac{\sum_{i=1}^Q [\alpha_F^i - \text{mean}(\alpha_F)]^2}{Q}} \quad (14)$$

In the same way, mean(α_R), and std(α_R) have been defined. Obviously, those error parameters depend both on the data set and on how matrices \underline{B} and \underline{A} have been estimated.

3.6. Experimental results

Examples of both matrix \underline{B} and matrix \underline{A} , calculated using a least-squares (LSM) procedure and a normalized (NLSM) one, are shown in (15), (16), (17) and (18). Regularities, as explained in section 3.4, are evident.

$$\underline{B}_{\text{LSM}} = \begin{pmatrix} -0.0049 & -0.0906 & 0.0431 \\ 0.1031 & 0.0028 & 0.0386 \\ 0.0058 & 0.1063 & 0.0436 \\ -0.0968 & 0.0133 & 0.0488 \end{pmatrix} \text{N}^{-1} \quad (15)$$

$$\underline{A}_{\text{LSM}} = \begin{pmatrix} 0.0038 & 5.3376 & 0.4412 & -4.6184 \\ -5.1023 & -0.2955 & 5.0369 & 0.2424 \\ 6.6381 & 5.6088 & 4.7730 & 5.9239 \end{pmatrix} \text{N} \quad (16)$$

$$\underline{B}_{\text{NLSM}} = \begin{pmatrix} -0.0048 & -0.0931 & 0.0429 \\ 0.1033 & -0.0018 & 0.0388 \\ 0.0052 & 0.1108 & 0.0442 \\ -0.0973 & 0.0180 & 0.0489 \end{pmatrix} \text{N}^{-1} \quad (17)$$

$$\underline{A}_{\text{NLSM}} = \begin{pmatrix} -0.2243 & 5.3036 & 0.6451 & -4.6032 \\ -4.9195 & -0.3092 & 4.8573 & 0.1728 \\ 6.6531 & 5.6167 & 4.7269 & 5.8884 \end{pmatrix} \text{N}. \quad (18)$$

Table 1 shows error parameters calculated applying LSM and NLSM to the sensor described in section 2. The two methods have been applied over the same data set. Solutions in the least-squares meaning ensure the best rms($\|\Delta X\|$), while, in general, normalized ones give better performances in terms of rms($\frac{\|\Delta X\|}{\|X\|}$), mean(α_X) and std(α_X).

4. Device hyperplane characterization method

4.1. Method description

Matrices $\underline{B}_{\text{LSM}}$ and $\underline{B}_{\text{NLSM}}$ reported in section 3.6 have rank 3, and so could not generate the whole \mathbb{R}^4 , but only a subspace of \mathbb{R}^4 having dimension 3. For example, by applying three force vectors directed along the principal axes to the matrix $\underline{B}_{\text{LSM}}$, the following fractional changes in resistance vectors would be obtained, considering a noiseless condition:

$$\begin{pmatrix} 0 \\ 0 \\ 0.1 \end{pmatrix} \text{N} \rightarrow \begin{pmatrix} 4.31 \\ 3.86 \\ 4.36 \\ 4.88 \end{pmatrix} \times 10^{-3} \quad (19)$$

$$\begin{pmatrix} 0.1 \\ 0 \\ 0 \end{pmatrix} \text{N} \rightarrow \begin{pmatrix} -0.49 \\ 10.31 \\ 0.58 \\ -9.68 \end{pmatrix} \times 10^{-3} \quad (20)$$

$$\begin{pmatrix} 0 \\ 0.1 \\ 0 \end{pmatrix} \text{N} \rightarrow \begin{pmatrix} -9.06 \\ 0.28 \\ 10.63 \\ 1.33 \end{pmatrix} \times 10^{-3}. \quad (21)$$

Furthermore, due to the physics of the considered sensor and to the *rank theorem* [13], in a noiseless environment, there is no force stimulus which would produce the following *fractional changes in resistance* vector (or multiples of it):

$$\begin{pmatrix} -0.5015 \\ 0.4836 \\ -0.5042 \\ 0.5103 \end{pmatrix} \times 10^{-3}. \quad (22)$$

This would mean applying a compression on two opposite piezoresistors (for example R_2 and R_4) and a traction on the other two (for example R_1 and R_3). Moreover, the *rank theorem* guarantees such a property: if the number of inputs to the sensor is three (the three force components) and there are no hidden inputs (or eventual hidden inputs remain constant), then the space which could be generated as an output from the sensor may have at most dimension 3 in \mathbb{R}^4 .

Observe that, as confirmed later by the experimental results in (31) and (32), this means that sensor outputs would be compelled to belong to an hyperplane. Such a hyperplane is characterized by its normal \underline{n} , and the vector of *fractional changes in resistance* reported in (22) is then a numerical estimation of this normal direction.

The main idea of the method described in this section, called the device hyperplane characterization method (DHCM), is to use the hyperplane constraint in order to reduce errors during the calibration phase, exploiting the point that the sensor output projection along \underline{n} is due to errors.

The DHCM is composed by the following steps:

- a great number of sensor outputs are gathered in order to characterize the hyperplane while unknown forces are applied;
- at least three forces are applied to the sensor and measured together with the corresponding sensor outputs;
- these last acquired sensor outputs are projected on the hyperplane;
- the sensor calibration matrices are obtained by fitting the applied forces and the projected data.

It is relevant to note that, as underlined in [3], data acquisition is time consuming for forces, but not for *fractional changes in resistance*. In order to measure the force that is applied to the sensor, a calibrated load cell [9] has to be used, taking care about its relative orientation with respect to the device under test (DUT). Moreover a coordinates transformation for forces from the calibrating unit reference system to that of the DUT is required. Measuring a *fractional changes in resistance* vector without knowing the applied force, instead, simply means using the conditioning electronics and the data acquisition system while loading the sensor with random stimuli. So, the most demanding operation in the DHCM is to measure simultaneously at least three force vectors and the related *fractional changes in resistance* vectors.

Before applying the regression, the hyperplane is characterized without taking care of the applied forces, considering the *fractional changes in resistance* $\underline{R}^1 \dots \underline{R}^Q$ obtained applying random stimuli and searching for the row vector $\underline{T} = [T_1 \ T_2 \ T_3]$ such that:

$$R_4^1 = \underline{T} \cdot \begin{pmatrix} R_1^1 \\ R_2^1 \\ R_3^1 \end{pmatrix} \quad \dots \quad R_4^Q = \underline{T} \cdot \begin{pmatrix} R_1^Q \\ R_2^Q \\ R_3^Q \end{pmatrix} \quad (23)$$

where R_i^j has the same meaning as in (7). The row vector \underline{T} can be obtained using a least-squares procedure (or, alternatively, a normalized least-squares one, as explained in section 3.3.2). For example, using a least-squares procedure, the result (see sections 3.3.1 and 3.3.3) is:

$$\underline{T} = (R_4^1 \ \dots \ R_4^Q) \cdot \begin{pmatrix} R_1^1 & \dots & R_1^Q \\ R_2^1 & \dots & R_2^Q \\ R_3^1 & \dots & R_3^Q \end{pmatrix}^\dagger \quad (24)$$

where \dagger represents the Moore–Penrose pseudoinversion.

The hyperplane is now characterized by the equation

$$T_1 \cdot R_1 + T_2 \cdot R_2 + T_3 \cdot R_3 - R_4 = 0. \quad (25)$$

The vector

$$\underline{m} = \begin{pmatrix} T_1 \\ T_2 \\ T_3 \\ -1 \end{pmatrix}$$

is orthogonal to the hyperplane.

The transformation described in equation (26) returns the vector \underline{n} , which is orthogonal to the hyperplane, and of unitary modulus.

$$\underline{n} = \frac{\underline{m}}{\|\underline{m}\|} = \frac{\underline{m}}{\sqrt{(T_1)^2 + (T_2)^2 + (T_3)^2 + (-1)^2}}. \quad (26)$$

Once the hyperplane is characterized and the vector \underline{n} obtained, if a certain *fractional changes in resistance* vector is measured, the experimental error is statistically reduced applying the transformation (27).

$$\underline{R}_{\text{proj}} = \underline{R}_{\text{meas}} - \underline{n} \cdot \underline{n}^T \cdot \underline{R}_{\text{meas}} = (\underline{I} - \underline{n} \cdot \underline{n}^T) \cdot \underline{R}_{\text{meas}}. \quad (27)$$

Observe that

- Equation (27) means that $\underline{M} = \underline{I} - \underline{n} \cdot \underline{n}^T$ is the matrix of the orthogonal projection of \mathbb{R}^4 on the hyperplane
- The matrix \underline{M} may be obtained using a wide data set, acquired without spending much time because it requires only *fractional changes in resistance* measurements.

As for the *shape from motion method* [3], for which only one force measurement is necessary, a reduced set of force measurements with respect to a traditional *least-squares procedure* is needed, but those few forces have to be measured in a very accurate way. For example, using the *shape from motion method*, if the measured force is accidentally scaled by a factor ρ , or rotated by an angle θ with respect to the really applied one, the calculated compliance matrix would be scaled by the same factor ρ , or rotated by θ . Something similar happens also for the proposed method, given that, if the number of *full measurements* decreases, the susceptibility to accidental errors increases, but, as pointed out later in section 4.4, a small number of good force acquisitions may ensure good results. Otherwise, if good force measures are not achievable, a wider set of trials could be applied, obtaining higher error rejection with respect to a traditional *least-squares procedure*, and achieving almost the same time consumption.

Table 2. Force and *fractional changes in resistance* error parameters using DHCM, as described in section 4.1.

	rms($\ \Delta \underline{F}\ $)	rms($\frac{\ \Delta \underline{F}\ }{\ \underline{F}\ }$)	mean($\ \Delta \underline{F}\ $)	mean($\frac{\ \Delta \underline{F}\ }{\ \underline{F}\ }$)	std($\ \Delta \underline{F}\ $)	std($\frac{\ \Delta \underline{F}\ }{\ \underline{F}\ }$)	mean(α_F)	std(α_F)
DHCM	0.0108 N	9.05%	0.009 18 N	7.35%	0.005 74 N	5.29%	3.18°	6.44°
	rms($\ \Delta \underline{R}\ $)	rms($\frac{\ \Delta \underline{R}\ }{\ \underline{R}\ }$)	mean($\ \Delta \underline{R}\ $)	mean($\frac{\ \Delta \underline{R}\ }{\ \underline{R}\ }$)	std($\ \Delta \underline{R}\ $)	std($\frac{\ \Delta \underline{R}\ }{\ \underline{R}\ }$)	mean(α_R)	std(α_R)
DHCM	0.001 52	9.05%	0.001 29	7.72%	0.000 808	4.72%	3.32°	4.57°

4.2. Hyperplane hypothesis validation parameters

In order to evaluate the robustness of DHCM, two other parameters with respect to those described in section 3.5 have been introduced. Given that, ideally, *fractional changes in resistance* vectors have to belong to the characteristic hyperplane of the sensor, hyperplane bond hypothesis and sensor linearity as well, are as much verified as the angle between each measured *fractional changes in resistance* vector and the estimated hyperplane is reduced. So, naming those angles β_R^i , $\text{mean}(\beta_R)$, and $\text{std}(\beta_R)$ have been considered, where symbols have the same meaning as in section 3.5. Results are shown in section 4.4.

4.3. Noise rejection properties

Given that the sensor is a redundant one, it has a certain noise immunity. Assuming that a linear relationship between input and output exists, and pretending that the characteristic hyperplane of the sensor is *a priori* known, measured *fractional changes in resistance* have to belong to that hyperplane. So, a real *fractional changes in resistance* measurement can be represented as the sum of an informative vector and a stochastic vector, having a certain probability density function. The informative vector has to belong to the characteristic hyperplane of the sensor, while noise may not have any privileged/forbidden direction in \mathbb{R}^4 . So, having an orthonormal family of 4×1 vectors $[\underline{v}_1, \underline{v}_2, \underline{v}_3]$, which generates the characteristic hyperplane of the sensor, and considering the vector \underline{n} defined in (26), which is normal to the hyperplane, each *fractional changes in resistance* measurement \underline{R}_m can be written as:

$$\begin{aligned} \underline{R}_m = & (a_1 + nde_1) \cdot \underline{v}_1 + (a_2 + nde_2) \cdot \underline{v}_2 \\ & + (a_3 + nde_3) \cdot \underline{v}_3 + (nde_4) \cdot \underline{n} \end{aligned} \quad (28)$$

where a_i are the informative coefficients, and nde_i (which are characterized by a certain joint probability density function) describe noise, disturbance and experimental error. Assuming that each nde_i has null mean, increasing the number of measurements during the characterization session reduces the error in calculating \underline{A} and \underline{B} with a least-squares method. The *device* hyperplane characterization method allows to increase the number of only *fractional changes in resistance* measurements without much time consumption. That way, having first characterized the hyperplane, sensor outputs noise belonging to the \underline{n} direction (in \mathbb{R}^4) is rejected using the projection (27) during the few (but 3 at least) force/*fractional changes in resistance* measurements. This already happens using a traditional least-squares method, but measurements have to be full ones (force and *fractional changes in resistance*), making the acquisition of a huge data set very expensive.

4.4. Experimental results

As shown in table 2, error parameters (defined in section 3.5, and refined in section 4.2) related to DHCM are almost equal to those obtained (see 1) using the least-squares procedures described in sections 3.3.1 and 3.3.2. We stress that in this approach the full data set was composed by only three force/*fractional changes in resistance* measurements. Moreover, for the reduced (only *fractional changes in resistance*, for hyperplane characterization) data set, the number of measurements was as high as that used previously in order to obtain \underline{B} and \underline{A} with a least-squares procedure. This way, there was a substantial saving of time for data acquisition, given that only *fractional changes in resistance* measurements were carried out applying a random force to the sensor (there was no need to take care with load cell alignment).

Matrices (33) and (34) obtained in such a way are very similar to (15), (17) and (16), (18), respectively. As stated in section 3.3.3, the calculated (35) projection matrix \underline{M} has the following properties:

$$\underline{A} \cdot \underline{M} = \underline{A} \quad (29)$$

$$\underline{M} = \underline{B} \cdot \underline{A} \quad (30)$$

Furthermore, the projection matrix \underline{M} has a null eigenvalue, related to the eigenvector which is orthogonal to the characteristic hyperplane of the sensor; all three other eigenvalues, related to eigenvectors belonging to the hyperplane, are 1 given that the projection on the hyperplane of a vector belonging to that subspace of \mathbb{R}^4 is the vector itself. As expected, matrix \underline{M} represents the identical application for vectors belonging to the hyperplane of the sensor. Finally, the hyperplane hypothesis is reasonably validated given that the absolute mean value and the standard deviation (defined in section 4.2) of the angle between *fractional changes in resistance* vectors and the characteristic hyperplane are less than 1° :

$$\text{mean}(\beta_R) = 0.506^\circ \quad (31)$$

$$\text{std}(\beta_R) = 0.195^\circ \quad (32)$$

Observe that, according to how angles have been defined, $\beta_R^i \geq 0 \forall i$, so it is normal for $\text{mean}(\beta_R)$ to be greater than zero.

$$\underline{B}_{\text{DHCM}} = \begin{pmatrix} -0.0050 & -0.0934 & 0.0425 \\ 0.1020 & -0.0043 & 0.0378 \\ 0.0056 & 0.1115 & 0.0445 \\ -0.0958 & 0.0223 & 0.0499 \end{pmatrix} \text{N}^{-1} \quad (33)$$

$$\underline{A}_{\text{DHCM}} = \begin{pmatrix} -0.3222 & 5.4247 & 0.8553 & -4.5970 \\ -4.9362 & -0.3323 & 4.7844 & 0.1841 \\ 6.7220 & 5.6122 & 4.6646 & 5.8968 \end{pmatrix} \text{N} \quad (34)$$

$$\underline{M}_{\text{DHCM}} = \begin{pmatrix} 0.74819 & 0.24226 & -0.25284 & 0.25648 \\ 0.24226 & 0.76693 & 0.24325 & -0.24676 \\ -0.25284 & 0.24325 & 0.74612 & 0.25754 \\ 0.25648 & -0.24676 & 0.25754 & 0.73875 \end{pmatrix} \quad (35)$$

5. Conclusions

A new calibration method for redundant linear force sensors has been proposed in this paper. The device hyperplane characterization method guarantees an accuracy which is similar to that achievable using traditional *least-squares methods* and is time effective, requiring, like the *shape from motion* method, only a few precise force measurements. This method is inspired by the *shape from motion method* [3, 5] and *collaborative calibration* [14] since it reduces the burden of data collection and considers sensor calibration as an output focused problem. Furthermore, according to the kind of sensor, it may require a simpler test bench with respect to *shape from motion*, given that there is no need for any geometrical bond for applied forces.

The results shown in this work may be improved, using better conditioning electronic circuitry, reducing the bandwidth of the output signals (for static characterization, only the DC value of each signal is needed), or applying a low/medium frequency sinusoidal supply voltage signal, instead of the DC polarization used here. That way, there would be no static polarization of the resistors, and the effect of flicker noise [15] would be reduced; each informative signal may be obtained using a differential amplifier followed by a demodulation system. That kind of conditioning electronic circuitry (similar to chopper [16] amplifiers or to DSB-SC modulators–demodulators) would not have particular limitations both for static and dynamic force sensing, and would increase the SNR (signal-to-noise ratio) with respect to the simpler one used in this work.

Finally, the method proposed here suggests a time effective geometrically inspired way for calculating calibration matrices, given that it is based on the hyperplane constraint, allowing rapid and precise calibration and real time monitoring of the proper functioning of the sensor. For instance, using relations (29) and (30) for \underline{M} , this method may also be used to check if the sensor is working properly in the case that some parameter (temperature, humidity, etc) variation affects \underline{M} . In fact, the evaluation of matrix \underline{M} can be performed while the sensor is working in its structured environment (artificial hand, prosthesis stump/socket interface, surgical instrument, etc) using a periodic automatic routine avoiding the application of a known force. This property may be used, in order to improve robustness and reliability of the calibrated sensor, as an alert system which would warn the user if the sensor is not working according to its model (properties (29) and (30) with respect to the previously calculated calibration matrices, eigenvectors of \underline{M} , etc), and eventually suggest recalibrating or replacing the sensor.

The authors are investigating also the possibility of using DHCM for slippage detection, as in [17], with the packaged tactile sensor described in [18] exploiting a mismatch, which occurs during slippage events, between the characteristic

hyperplane of the inner sensor and *fractional changes in resistance* vectors. That way, using such a system, only output readings would be necessary for slippage detection, without the need for preliminary calibration, given that hyperplane characterization is an output-only problem.

Acknowledgments

The silicon force sensor realization has been supported by the European Commission's Improving Human Potential (IHP) Program in collaboration with the Institut für Mikrotechnik Mainz (IMM), Germany. The authors would like to gratefully thank Professor Mario Poletti, from Department of Applied Mathematics 'Ulisse Dini', University of Pisa, whose advice was fundamental for the development and formalization of DHCM, and Professor Giovanni Basso, belonging to Department of Information Engineering, University of Pisa, for valuable discussions.

References

- [1] Berkelman P J, Whitcomb L L, Taylor R H and Jensen P 2003 A miniature microsurgical instrument tip force sensor for enhanced force feedback during robot-assisted manipulation *IEEE Trans. Robot. Autom.* **19** 917–21
- [2] Chang Y H, Huang Y C, Liu Y P and Tsay S M 1998 A novel structural design for force/torque fingertip sensors *Meas. Sci. Technol.* **9** 1196–203
- [3] Voyles R, Morrow J and Khosla P 1997 The shape from motion approach to rapid and precise force/torque sensor calibration *J. Dyn. Syst. Meas. Control* **119** 229–35
- [4] Wang L and Beebe D J 2000 A silicon-based shear force sensor: development and characterization *Sensors Actuators A* **84** 33–44
- [5] Sun Y, Kim K, Voyles R and Nelson B 2006 Calibration of multi-axis MEMS force sensors using the shape from motion method *IEEE Int. Conf. Robot. Autom. (May)* vol 1
- [6] Park Jae jun, Kwon Kihwan and Cho Nahngyoo 2006 Development of a coordinate measuring machine (cmm) touch probe using a multi-axis force sensor *Meas. Sci. Technol.* **17** 2380–6
- [7] Bicchi A 1990 A criterion for optimal design of multi-axis force sensors *AIM-1263*
- [8] Beccai L, Roccella S, Arena A, Valvo F, Valdastrì P, Menciassi A, Carrozza M C and Dario P 2005 Design and fabrication of a hybrid silicon three-axial force sensor for biomechanical applications *Sensors Actuators A* **120** 370–82
- [9] Valdastrì P, Roccella S, Beccai L, Cattin E, Menciassi A, Carrozza M C and Dario P 2005 Characterization of a novel hybrid silicon three-axial force sensor *Sensors Actuators A* **123** 249–57
- [10] Suhling J C and Jaeger R C 2001 Silicon piezoresistive stress sensors and their application in electronic packaging *Sensors J.* **1** 14–30
- [11] Shan J H, Mei T, Sun L, Kong D Y, Zhang Z Y, Ni L, Meng M and Chu J R 2005 The design and fabrication of a flexible three-dimensional force sensor skin *2005 IEEE/RSJ Int. Conf. on Intelligent Robots and Systems*
- [12] Beccai L 2003 Design, fabrication and packaging of a silicon based three-axial force sensor for biomedical application *PhD Thesis* Microsystem Engineering, Università degli Studi di Roma 'Tor Vergata'. XV cycle
- [13] Tomasi C and Kanade T 1991 Shape and motion from image streams: a factorization method *Technical Report* CMU-CS-91-172, Carnegie Mellon University, Pittsburgh, PA

- [14] Voyles R and Khosla P 1997 Collaborative calibration: extending shape from motion calibration *IEEE Int. Conf. Robot. Autom. (April)* vol 4 pp 2795–800
- [15] Harkey J A and Kenny T W 2000 $1/f$ noise considerations for the design and process optimization of piezoresistive cantilevers *J. Microelectromech. Syst.* **9** 226–35
- [16] Enz C C and Temes G C 1996 Circuit techniques for reducing the effects of op-amp imperfections: autozeroing, correlated double sampling, and chopper stabilization *Proc. IEEE* **84** 1584–614
- [17] Cranny A, Cotton D P J, Chappell P H, Beeby S P and White N M 2005 Thick-film force, slip and temperature sensors for a prosthetic hand *Meas. Sci. Technol.* **16** 931–41
- [18] Beccai L, Roccella S, Ascari L, Valdastrì P, Sieber A, Carrozza M C and Dario P 2006 Experimental analysis of a soft compliant tactile microsensor to be integrated in an anthropomorphic artificial hand *Proc. ESDA2006 8th Biennial ASME Conf. on Engineering Systems Design and Analysis (July)* vol ESDA2006